[Electronic Supplementary Information (ESI)]

Time-Resolved X-ray Crystal Structure Analysis for Elucidating the Hidden 'Over-Neutralized' Phase of TTF-CA

Manabu Hoshino,[*] Shunsuke Nozawa, Tokushi Sato, Ayana Tomita, Shin-ichi Adachi, and Shin-ya Koshihara

General experiment. Black suitable single crystals of TTF-CA were grown by the cosublimation of TTF and CA. The single crystal of dimensions $0.13 \times 0.10 \times 0.07$ mm was used for the experiment. All diffraction data were collected using a marCCD X-ray detector on beamline NW14A of the Photon Factory Advanced Ring (PF-AR) at the High Energy Accelerator Research Organization (Tsukuba, Japan). Monochromatic X-ray pulses ($\lambda = 0.56366$ Å; Si(111) double crystals) were synchronized with femtosecond laser pulses. For synchronization, the frequency of the X-rays from the PF-AR was reduced to 946 Hz using an X-ray pulse selector. The sample temperature was controlled with a cold nitrogen stream from an Oxford cryogenic system. Photograph for the experimental setup is shown in Supplementary Figure S2. Time-resolved X-ray diffraction experiments were performed at 90 K. Light-on and light-off diffraction data frames were alternately collected to minimize systematic errors. Under the present laser power conditions (< 10 mJ cm^{-2}), no significant photoinduced appearance of $0k0$ ($k =$ odd) reflections was recorded at any delay time. The reflections are absent in the N phase (the suggested crystallographic space group: $P2_1/n$) but are present in the I phase (Pn). The absence of the reflections indicated that the photoinduced NI transition was deactivated within a much shorter time than the pulse width of the X-ray radiation. Additionally, static X-ray diffraction experiments without laser irradiation were performed at 100 K. All crystal structures were solved by direct methods (*SHELXS-97*) and refined by the full-matrix least-squares method (*SHELXL-97*) (Ref. S1). All the non-hydrogen atoms were refined anisotropically. All the hydrogen atoms were refined isotropically using $U_{iso} = 1.2U_{eq}$ of the connected carbon atom.

Sample quality was checked by drawing a photo-difference Fourier map at the first delay point ($\Delta t = 150$ ps). If a poor-quality crystal was selected for measurement, the noise of the map increased and became high. One of the results is shown in Supplementary Figure S3. Although the height and depth of the peak densities were almost the same as those described in the main manuscript (ca. ± 0.25 eÅ^{-3}), the noise level was almost the same as that of the peaks, indicating that the peak height and depth depended on the excitation power and data fluctuation because the sample quality was reflected in the noise density of the map.

General crystallographic data. Refined formula: $C_6H_4S_4$ and $C_6O_2Cl_4$, formula weight (M_r): 450.19, crystal system: monoclinic, $Z = 2$.

Crystallographic data at $\Delta t = 150$ ps (On150ps) and its light-off condition

(Off150ps). On150ps: 11104 unique reflections merged from 46260 recorded ones ($3.77 < \theta < 33.56°$) were used for structural analysis (R_{int} = 0.0330). Lattice parameters, R-factor on $F^2 > 2\sigma(F^2)$, and weighted R-factor are follows: a = 7.2140(1) Å, b = 7.5870(1) Å, c = 14.4850(1) Å, β = 99.1310(2)°, V = 782.756(16) Å^3, R = 0.0209, wR = 0.0593, S = 1.081. Calculated density is 1.910. Linear absorption coefficient (μ) is 0.654. Residual electron density (max/min) is 0.721/–0.413 eÅ^{-3}. Off150ps: 11103 unique reflections merged from 46254 recorded ones ($3.77 < \theta < 33.55°$) were used for structural analysis (R_{int} = 0.0326). Lattice parameters, R-factor on $F^2 > 2\sigma(F^2)$, and weighted R-factor are follows: a = 7.2130(1) Å, b = 7.5860(1) Å, c = 14.4840(1) Å, β = 99.1270(3)°, V = 782.499(16) Å^3, R = 0.0206, wR = 0.0587, S = 1.082. Calculated density is 1.911. Linear absorption coefficient (μ) is 0.654. Residual electron density (max/min) is 0.701/–0.487 eÅ^{-3}.

Crystallographic data at Δt = 500 ps (On500ps) and its light-off condition (Off500ps). On500ps: 11111 unique reflections merged from 46185 recorded ones ($3.77 < \theta < 33.55°$) were used for structural analysis (R_{int} = 0.0342). Lattice parameters, R-factor on $F^2 > 2\sigma(F^2)$, and weighted R-factor are follows: a = 7.2140(1) Å, b = 7.5870(1) Å, c = 14.4850(1) Å, β = 99.1300(3)°, V = 782.758(16) Å^3, R = 0.0209, wR = 0.0595, S = 1.089. Calculated density is 1.910. Linear absorption coefficient (μ) is 0.654. Residual electron density (max/min) is 0.737/–0.443 eÅ^{-3}. Off500ps: 11099 unique reflections merged from 46232 recorded ones ($3.77 < \theta < 33.54°$) were used for structural analysis (R_{int} = 0.0329). Lattice parameters, R-factor on $F^2 > 2\sigma(F^2)$, and weighted R-factor are follows: a = 7.2130(1) Å, b = 7.5860(1) Å, c = 14.4840(1) Å, β = 99.1250(3)°, V = 782.503(16) Å^3, R = 0.0210, wR = 0.0603, S = 1.097. Calculated density is 1.911. Linear absorption coefficient (μ) is 0.654. Residual electron density (max/min) is 0.723/–0.457 eÅ^{-3}.

Crystallographic data at Δt = 800 ps (On800ps) and its light-off condition (Off800ps). On800ps: 11101 unique reflections merged from 46028 recorded ones ($3.77 < \theta < 33.55°$) were used for structural analysis (R_{int} = 0.0326). Lattice parameters, R-factor on $F^2 > 2\sigma(F^2)$, and weighted R-factor are follows: a = 7.2140(1) Å, b = 7.5870(1) Å, c = 14.4850(1) Å, β = 99.1300(3)°, V = 782.758(16) Å^3, R = 0.0207, wR = 0.0583, S = 1.078. Calculated density is 1.910. Linear absorption coefficient (μ) is 0.654. Residual electron density (max/min) is 0.698/–0.513 eÅ^{-3}. Off800ps: 11112 unique reflections merged from 46021 recorded ones ($3.77 < \theta < 33.57°$) were used for structural analysis (R_{int} = 0.0323). Lattice parameters, R-factor on $F^2 > 2\sigma(F^2)$, and

weighted R-factor are follows: $a = 7.2120(1)$ Å, $b = 7.5860(1)$ Å, $c = 14.4830(1)$ Å, $\beta = 99.1270(3)°$, $V = 782.336(16)$ Å^3, $R = 0.0207$, $wR = 0.0595$, $S = 1.081$. Calculated density is 1.911. Linear absorption coefficient (μ) is 0.655. Residual electron density (max/min) is 0.736/–0.484 eÅ^{-3}.

Crystallographic data at $\Delta t = 1$ ns (On1ns) and its light-off condition (Off1ns). On1ns: 11106 unique reflections merged from 46004 recorded ones ($3.77 < \theta < 33.56°$) were used for structural analysis ($R_{int} = 0.0327$). Lattice parameters, R-factor on $F^2 > 2\sigma(F^2)$, and weighted R-factor are follows: $a = 7.2140(1)$ Å, $b = 7.5870(1)$ Å, $c = 14.4850(1)$ Å, $\beta = 99.1320(3)°$, $V = 782.753(16)$ Å^3, $R = 0.0207$, $wR = 0.0587$, $S = 1.081$. Calculated density is 1.910. Linear absorption coefficient (μ) is 0.654. Residual electron density (max/min) is 0.701/–0.505 eÅ^{-3}. Off1ns: 11084 unique reflections merged from 46099 recorded ones ($3.77 < \theta < 33.55°$) were used for structural analysis ($R_{int} = 0.0316$). Lattice parameters, R-factor on $F^2 > 2\sigma(F^2)$, and weighted R-factor are follows: $a = 7.2120(1)$ Å, $b = 7.5860(1)$ Å, $c = 14.4830(1)$ Å, $\beta = 99.1270(3)°$, $V = 782.336(16)$ Å^3, $R = 0.0204$, $wR = 0.0581$, $S = 1.087$. Calculated density is 1.911. Linear absorption coefficient (μ) is 0.655. Residual electron density (max/min) is 0.668/–0.450 eÅ^{-3}.

Crystallographic data at 100 K (Heated). 11130 unique reflections merged from 46042 recorded ones ($3.77 < \theta < 33.55°$) were used for structural analysis ($R_{int} = 0.0324$). Lattice parameters, R-factor on $F^2 > 2\sigma(F^2)$, and weighted R-factor are follows: $a = 7.2220(1)$ Å, $b = 7.5910(1)$ Å, $c = 14.4930(1)$ Å, $\beta = 99.1370(2)°$, $V = 784.457(16)$ Å^3, $R = 0.0213$, $wR = 0.0600$, $S = 1.089$. Calculated density is 1.906. Linear absorption coefficient (μ) is 0.653. Residual electron density (max/min) is 0.793/–0.390 eÅ^{-3}.

Detailed method for drawing the photo-difference Fourier maps. To draw photo- and thermal-difference Fourier maps, changes of the overall temperature factor (ΔB) were estimated by the Wilson-type plot.(Ref. S2) The results of the Wilson-type plots are shown in Supplementary S4. The slope of the liner fit to the Wilson-type plot corresponds to $\Delta B/2$. The obtained ΔB values were used as a correction term to $F_{o(light\text{-}off)}$ and $F_{o(90\ K)}$ in the following equation:

$$F'_o = k \exp(-\Delta B \sin^2\theta/\lambda^2)\, F_o$$

where F'_o is the corrected F_o and k is the overall scale factor. The ΔB values are follows: 0.0254 (for $F_{o(light\text{-}off)}$ at $\Delta t = 150$ ps), 0.0101 ($\Delta t = 500$ ps), 0.0131 ($\Delta t = 800$

ps), 0.0221 (Δt = 1 ns), and 0.0714 (for $F_{o(90\ K)}$). Photoinduced geometrical changes in a few percent of the species in the crystal were reflected in this map (Ref. 23 in the main manuscript and Ref. S3).

All F_o sets were obtained as an output of crystal structure refinement. The difference Fourier synthesis was performed using the usual Fourier synthesis equation with $F_{o(light-on)} - F_{o(light-off)}$ as its coefficient. The lattice parameters and phases at the light-off condition were used in the synthesis. Based on those map, population of photoinduced species generated in the crystal was estimated by refinement of a disordered model. The positions and displacement parameters of the initial molecule was constrained and the positions of the disordered Cl19 and Cl25, which showed displacement change at all delay points, were refined with same displacement parameters as the initial one (using the same method as Ref. 23). From that analysis, about 1% was estimated as population of photo-converted species. The C15=O18 and C21=O24 bonds were shortened upon reaching the over-neutralized phase (at Δt = 800 ps). The shrinks were respectively 1.226(4) → 1.222(13) Å and 1.221(4) → 1.217(13) Å. These findings suggested a 4 × 10^{-3} Å shortening of the C=O bond, but the standard uncertainty associated with these values was larger than their differences because of the very small population of photoinduced species (1%). If the ρ value became 0.00 by the over-neutralization, the C=O shortening would be approximately 8 × 10^{-3} Å (estimated from the theoretically reported C=O lengths at ρ = 0.25 and 0.00 in Ref. S4). We therefore considered that the observed C=O shortening was qualitative in nature.

All C–Cl bonds were also shortened accompanying with the over-neutralization. Two-dimensional photo-difference Fourier maps representing C=O and C–Cl shortenings were shown in Supplementary Figure S5. The shrinks of C16–Cl19, C17–Cl20, C22–Cl25 and C23–Cl26 at Δt = 800 ps were respectively 1.721(3) → 1.711(13) Å, 1.698(3) → 1.671(13) Å, 1.694(3) → 1.687(13) Å and 1.713(3) → 1.781(13) Å. In theoretical calculations, the 7 × 10^{-3} Å shortening of C–Cl with decreasing of ρ from 0.25 to 0.00 was reported (Ref. 30). The shortenings of C16–Cl19 and C22–Cl25 were also within experimental errors, but qualitatively represent the over-neutralization of TTF-CA. The shortenings of C17–Cl20 and C23–Cl26 relatively significant compared to others. The reason of it is guessed the atomic fluctuation shown at Δt = 150 ps and 1 ns was somewhat affected to the positions of Cl20 and Cl26.

The observed structural change by over-neutralization was very small and not accompanying with change of the extinction rule. Therefore, discuss about intensity change of some selected reflections would be an arbitrary way. On the other hand, photo-difference Fourier map is based on intensity change of all recorded reflections.

Hence, drawing the photo-difference Fourier maps was selected for objectively and directly discuss about the photoinduced structural change.

Decreased value of ρ ($\Delta\rho$) was estimated based on the ratio between the C=O or C–Cl shortening and the above theoretically proposed value. For this estimation, the linear approximate equation based on the reported relation between ρ and C=O or C–Cl lengths in ref. 30 was used. The former was −0.13 and the latter was −0.25. Therefore, $\Delta\rho$ was roughly estimated as at least −0.1.

The reliability of the photo-difference Fourier maps were evaluated based on the error map, which synthesized using the difference of two light-off datasets ($F_{o(\text{light-off 1st})} - F_{o(\text{light-off 2nd})}$) on the same crystal and the measurement temperature (90 K). Almost all electron density in the map was within ±0.1 eÅ^{-3} (Supplementary Figure S6). Therefore, electron densities greater than ±0.1 eÅ^{-3}, drawn in Fig. 2a, are properly describing the photoinduced structural change.

The shortening of C–S and the central C=C in TTF upon the over-neutralization is also expected (Refs. 29 and S5). However, because of the C–S shortenings are expected smaller than the C=O and C–Cl shortenings in CA (Ref. 29), those shortenings were considered as too small to appear in the photo-difference Fourier map. Regarding the C=C shortening, very small (lower than the error density level) difference electron densities corresponding to the C=C shortening were appeared in the photo-difference Fourier map (Supplementary Figure S7). Additionally, increment of bonding electron densities due to the bond shortening was also appeared around the center of C=C. Those suggested the C=C shortening upon the over-neutralization.

Explanation of crystal structure analysis under the *Pn* condition. The intermolecular distance between TTF and CA in the 1D column is discussed based on the C2···C15 and C9···C21 distances, which are defined as a intra and interdimer distance in the *I* phase by García et al.(Ref. 29) All of C2···C15 and C9···C21 distances are tabled in Supplementary Table S1. At the light-off stages, differences between C2···C15 and C9···C21 are larger than three times of its standard deviation. That indicates the weak charge-transfer dimers are generated in the *N* phase. These dimers represent the ρ of the *N* phase ($\rho \sim 0.3$). Those small differences between intra and interdimer distances do not contribute significant intensity of *0k0* reflections. Therefore, the space group of TTF-CA was suggested as *P2$_1$/n* based on the statistics of collected diffraction data. However, geometrical features described above and the reported ρ value at the *N* phase indicates the two-fold screw axis (in other word, the inversion center on which TTF and CA lie) is pseudo-symmetry and *Pn* is more suitable space

group for TTF-CA.

During the structure refinement process, atomic displacement parameters between the pseudo-symmetrically related atoms were constrained as being identical to avoid any severe parameter interaction.

The pseudo-symmetry caused a sort of problem in the photo-difference Fourier map. In the error map using the structural factors at the $P2_1/n$ condition, serious noise densities appeared on some atoms in it (Supplementary Figure S8). Those noise densities would be due to the mergence of reflections correlated with the pseudo-inversion center. R_{int} is one of criteria for justify adequacy of the mergence. R_{int} at the Pn condition is lower than at the $P2_1/n$ conditions for all dataset (Supplementary Table S2). That indicates the mergence of reflections correlated with the pseudo-inversion center decrease the quality of dataset and would cause large noise density in the photo-difference Fourier map.

Examination of thermal equilibrium at the light-on stage. The thermal equilibrium in the current case was complicated because the observed structural dynamics represented a non-equilibrium phenomenon in the relaxation process from the photoinduced *I* phase. In the current study, the thermal equilibrium was examined from the perspective of sample temperature by the comparison of the atomic displacement parameters (ADP) during the all light-on stages. The ADP was one of thermal parameters and was typically used in discussions centering on the sample temperature. The ADP of CA was appeared constant at all the light-on stages. However, atomic fluctuation, which shown in the photo-difference Fourier maps, would be included in those. The ADP of TTF was therefore used for this comparison. All of the ADP values of TTF are tabulated in Supplementary Table S3. During all the light-on stages, the ADP remained almost entirely within their experimental error ranges. The sample had therefore reached thermal equilibrium (equilibrium temperature in a precise sense) between $\Delta t = 150$ ps and 1 ns.

Reproducibility experiment. The single crystal of TTF-CA with dimensions $0.21 \times 0.09 \times 0.06$ mm was used for the experiment. Same experimental condition, except for X-ray wavelength ($\lambda = 0.68889$ Å was used), was applied. Photo-difference Fourier maps are shown in Supplementary Figure S9. The least-square refinement of photoinduced species at $\Delta t = 800$ ps qualitatively indicate approximately -0.01 Å shortening of C=O and C–Cl. Those reproducible results strongly assure the over-neutralization phenomenon.

a) Photoinduced bending

hv

Light-ON   Light-OFF

Electron density

Photo-difference
Fourier map

b) Photoinduced increment of ADP

hv

Light-OFF

Light-ON

Electron density

Photo-difference
Fourier map

*In this study, outer positive electron
density was smaller than noise density
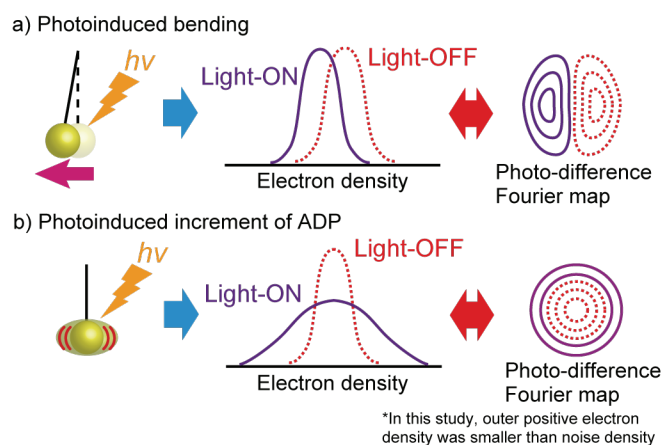
Figure S1. Schematic drawings for understanding of photo-difference electron densityies. (a) Photoinduced bending, (b) Photoinduced increment of ADP.
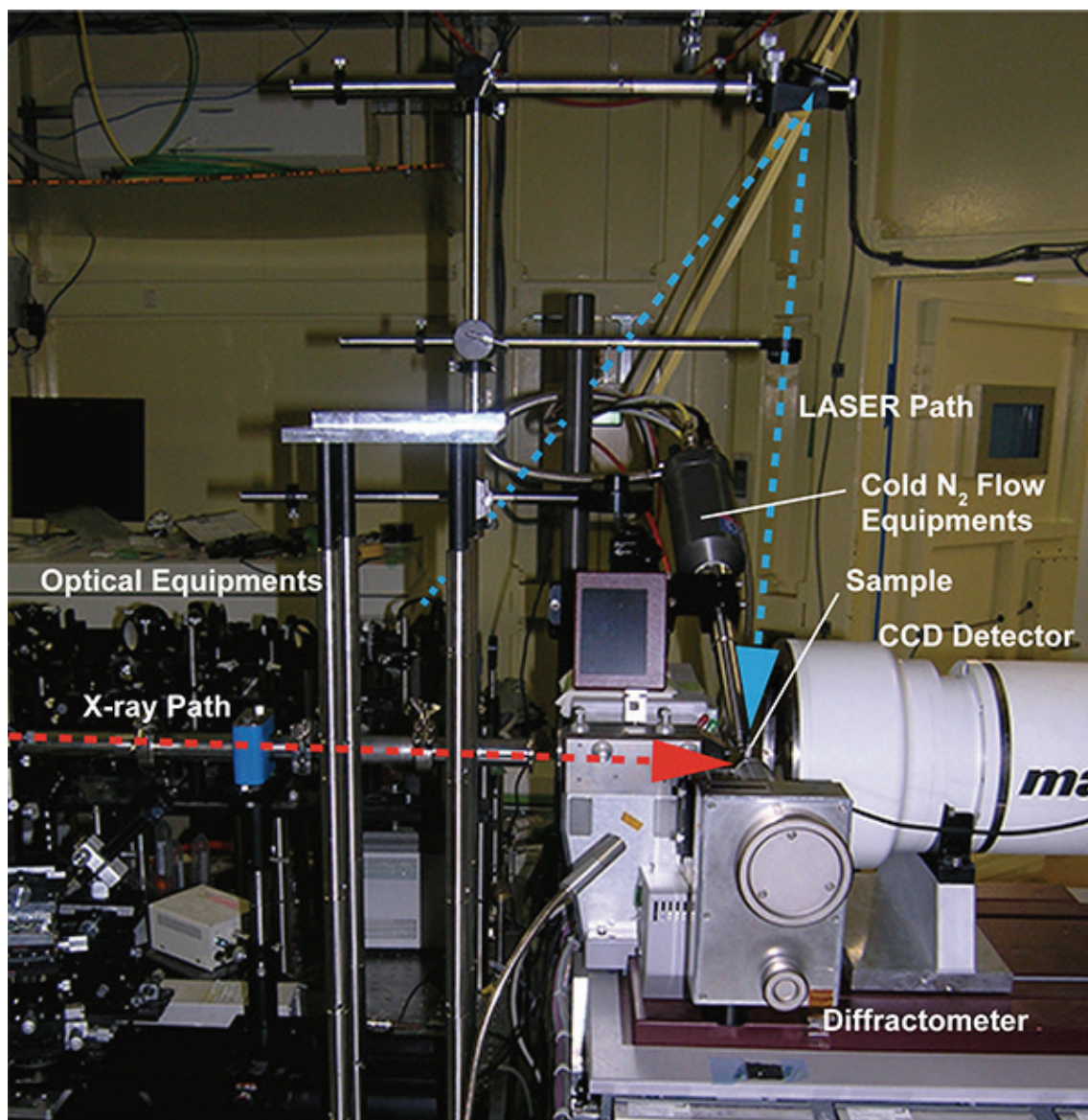
Figure S2. Photograph for the experimental setup at PF-AR NW14A in KEK. Excitation laser light irradiated from the vertical direction to the sample position.
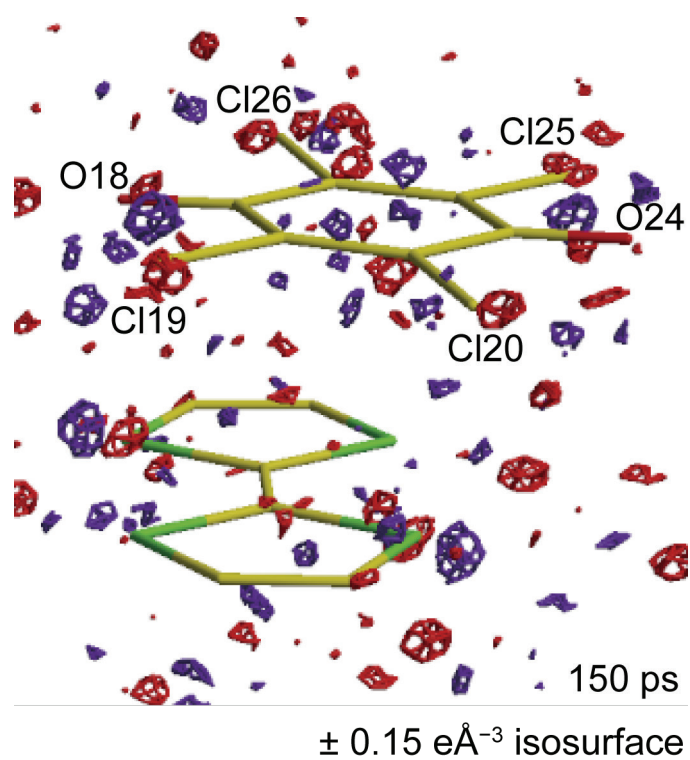
± 0.15 eÅ^{-3} isosurface

Figure S3. Photo-difference Fourier map using a poor-quality crystal. Purple and red surfaces (±0.15 eÅ^{-3} isosurfaces) denote positive and negative electron densities, respectively.
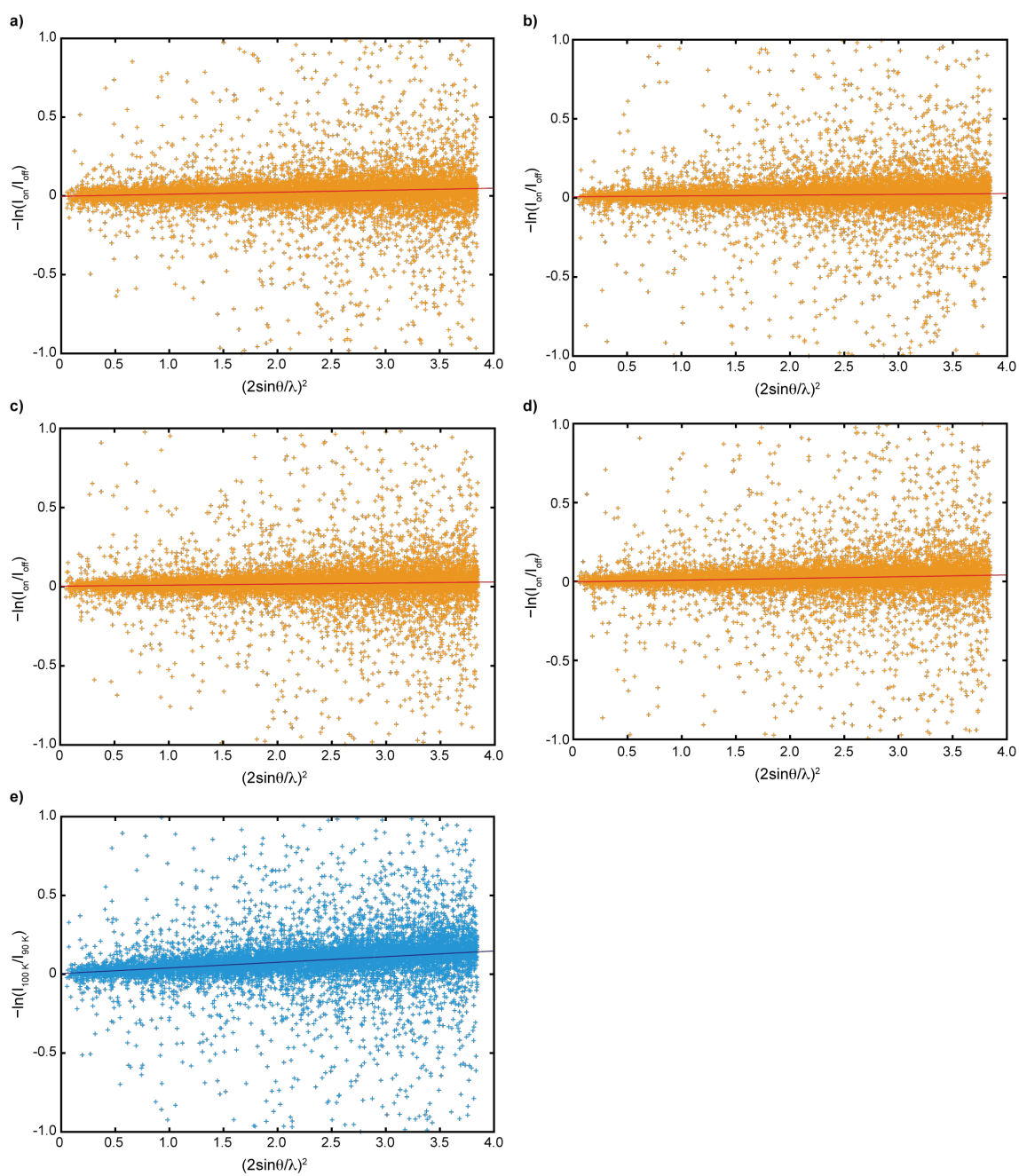
Figure S4. Wilson-type plots. Wilson type plots for the correction of $F_{o(\text{light-off})}$ at Δt = 150 ps (**a**), 500 ps (**b**), 800 ps (**c**), 1 ns (**d**), and $F_{o(90\ K)}$ (**e**). Red and Blue solid lines are the liner fitted functions.
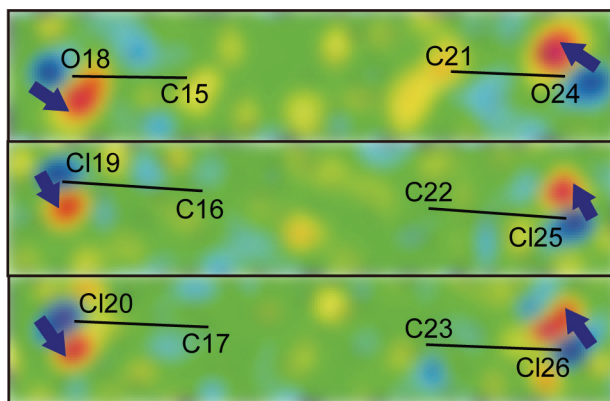
Figure S5. Two-dimensional photo-difference Fourier maps at $\Delta t = 800$ **ps.** All maps are drawn perpendicular to the mean plane of CA. Blue arrows indicate the positional change of O and Cl upon over-neutralization. Electron density max (blue)/min (red) = $0.14/-0.14$ eÅ^{-3} in all maps. These maps indicate the positional change upon over-neutralization is concerned with not only rotation (direction perpendicular to the bond) but also shortening (direction along to the bond).
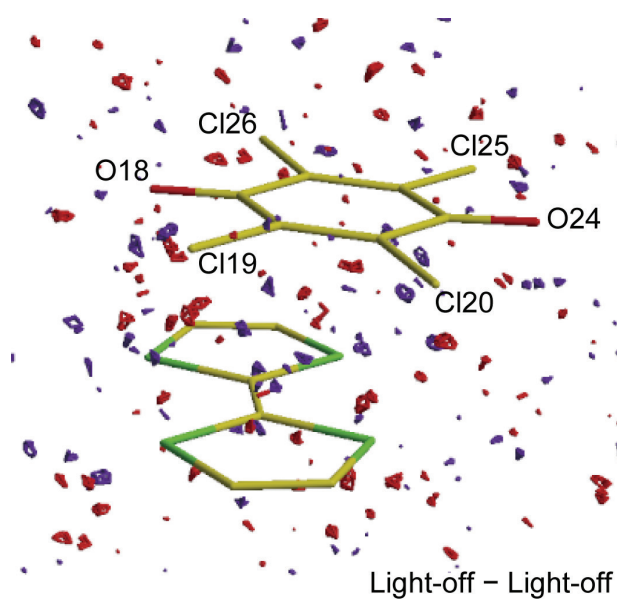
Figure S6. The error map drawn using the $F_{o(\text{light-off 1st})} - F_{o(\text{light-off 2nd})}$ coefficient. Purple and red surfaces (± 0.1 eÅ^{-3} isosurfaces) denote positive and negative electron densities, respectively.
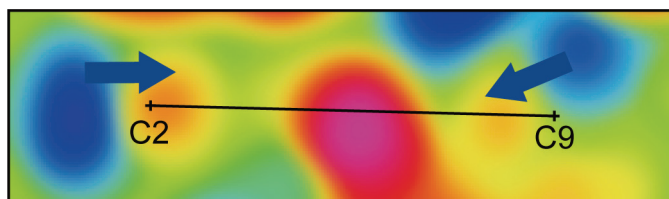
Figure S7. Photo-difference Fourier map around the central C=C in TTF at Δt = 800 ps. Blue arrows indicate the positional change of C upon over-neutralization. Electron density max (blue)/min (red) = $0.05/-0.05$ $e\text{Å}^{-3}$. The map was drawn perpendicular to the mean plane of TTF.

Table S1 C9···C21* and C2···C15 distances in the 1D column of TTF and CA and differences of them

	C9···C21 / Å	C2···C15 / Å	(C9···C21) – (C2···C15) / Å
Off150ps	3.379(4)	3.345(4)	+0.034(6)
On150ps	3.377(5)	3.349(5)	+0.028(7)
Off500ps	3.374(5)	3.352(5)	+0.022(7)
On500ps	3.361(5)	3.366(5)	−0.005(7)**
Off800ps	3.373(5)	3.352(5)	+0.021(7)
On800ps	3.362(5)	3.366(5)	−0.004(7)**
Off1ns	3.379(5)	3.347(5)	+0.032(7)
On1ns	3.376(5)	3.352(5)	+0.024(7)
Heated	3.379(5)	3.356(5)	+0.023(7)

* Its position is moved by the symmetric operation: $1 - x$, $1 - y$, $-z$.

** Differences at these delay point suggest the equally stacking in the 1D column. These structural changes were not observed in the photo-difference map. But the averaged structure suggests over-neutralization clarified in this study.

Light-off − Light-off (*P2₁*/*n*)
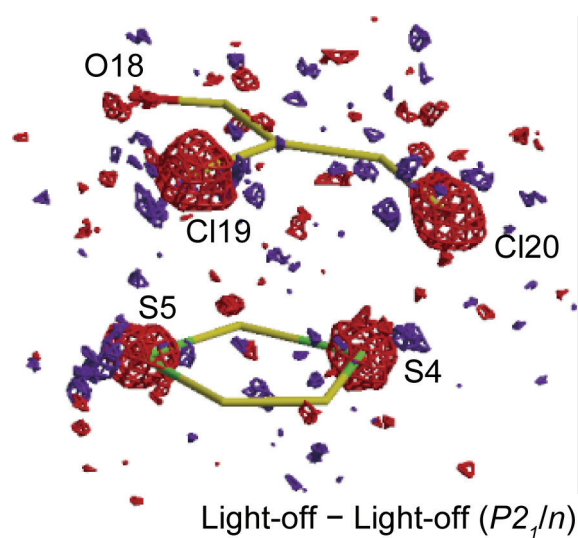
Figure S8. The error map at the *P2₁*/*n* condition. Asymmetric fragments of TTF and CA in *P2₁*/*n* are drawn. Purple and red surfaces (± 0.1 eÅ^{-3} isosurfaces) denote positive and negative electron densities, respectively.

**Table S2 R_{int} obtained under the *Pn* and *P2₁/n* conditions**

	Pn	*P2$_1$/n*
Off150ps	0.0326	0.0343
On150ps	0.0330	0.0349
Off500ps	0.0329	0.0345
On500ps	0.0342	0.0358
Off800ps	0.0323	0.0339
On800ps	0.0326	0.0344
Off1ns	0.0316	0.0334
On1ns	0.0327	0.0346

Table S3 All Atomic displacement parameters (Å^2)

	U^{11}	U^{22}	U^{33}	U^{12}	U^{13}	U^{23}
Off150ps						
S4	0.01039 (3)	0.00446 (4)	0.00683 (3)	−0.00162 (2)	0.00146 (2)	0.00115 (2)
S5	0.00770 (3)	0.00709 (4)	0.00505 (3)	−0.00060 (2)	0.00120 (2)	0.00081 (2)
S11	0.01039 (3)	0.00446 (4)	0.00683 (3)	−0.00162 (2)	0.00146 (2)	0.00115 (2)
S12	0.00770 (3)	0.00709 (4)	0.00505 (3)	−0.00060 (2)	0.00120 (2)	0.00081 (2)
C1	0.00848 (14)	0.00595 (14)	0.01030 (12)	−0.00108 (9)	0.00191 (10)	−0.00200 (9)
C2	0.01038 (12)	0.00481 (13)	0.00545 (11)	−0.00168 (9)	0.00111 (8)	0.00058 (8)
C3	0.00817 (15)	0.0079 (2)	0.00808 (11)	0.00008 (12)	0.00138 (11)	−0.00274 (11)
C8	0.00848 (14)	0.00595 (14)	0.01030 (12)	−0.00108 (9)	0.00191 (10)	−0.00200 (9)
C9	0.01038 (12)	0.00481 (13)	0.00545 (11)	−0.00168 (9)	0.00111 (8)	0.00058 (8)
C10	0.00817 (15)	0.0079 (2)	0.00808 (11)	0.00008 (12)	0.00138 (11)	−0.00274 (11)
Cl19	0.01022 (3)	0.01222 (4)	0.00403 (3)	−0.00231 (2)	0.00042 (2)	0.00085 (2)
Cl20	0.00942 (3)	0.00571 (4)	0.00864 (3)	−0.00256 (2)	0.00097 (2)	−0.00097 (2)
Cl25	0.01022 (3)	0.01222 (4)	0.00403 (3)	−0.00231 (2)	0.00042 (2)	0.00085 (2)
Cl26	0.00942 (3)	0.00571 (4)	0.00864 (3)	−0.00256 (2)	0.00097 (2)	−0.00097 (2)
O18	0.01525 (12)	0.00711 (12)	0.00777 (9)	−0.00273 (8)	0.00401 (8)	0.00273 (7)
O24	0.01525 (12)	0.00711 (12)	0.00777 (9)	−0.00273 (8)	0.00401 (8)	0.00273 (7)
C15	0.00831 (12)	0.00513 (15)	0.00552 (10)	−0.00078 (9)	0.00216 (8)	0.00115 (9)
C16	0.00770 (12)	0.00634 (13)	0.00451 (9)	−0.00107 (9)	0.00149 (8)	0.00061 (8)
C17	0.00717 (11)	0.00503 (13)	0.00532 (13)	−0.00124 (8)	0.00156 (9)	0.00018 (9)
C21	0.00831 (12)	0.00513 (15)	0.00552 (10)	−0.00078 (9)	0.00216 (8)	0.00115 (9)
C22	0.00770 (12)	0.00634 (13)	0.00451 (9)	−0.00107 (9)	0.00149 (8)	0.00061 (8)
C23	0.00717 (11)	0.00503 (13)	0.00532 (13)	−0.00124 (8)	0.00156 (9)	0.00018 (9)
On150ps						
S4	0.01063 (3)	0.00467 (4)	0.00707 (3)	−0.00163 (2)	0.00148 (2)	0.00121 (2)
S5	0.00793 (3)	0.00739 (4)	0.00527 (3)	−0.00060 (2)	0.00122 (2)	0.00082 (2)
S11	0.01063 (3)	0.00467 (4)	0.00707 (3)	−0.00163 (2)	0.00148 (2)	0.00121 (2)
S12	0.00793 (3)	0.00739 (4)	0.00527 (3)	−0.00060 (2)	0.00122 (2)	0.00082 (2)
C1	0.00882 (13)	0.00630 (14)	0.01073 (12)	−0.00110 (9)	0.00200 (9)	−0.00209 (9)
C2	0.01053 (12)	0.00497 (13)	0.00571 (10)	−0.00168 (8)	0.00111 (8)	0.00055 (8)
C3	0.00829 (17)	0.0083 (2)	0.00824 (13)	0.00014 (13)	0.00124 (12)	−0.00281 (12)
C8	0.00882 (13)	0.00630 (14)	0.01073 (12)	−0.00110 (9)	0.00200 (9)	−0.00209 (9)
C9	0.01053 (12)	0.00497 (13)	0.00571 (10)	−0.00168 (8)	0.00111 (8)	0.00055 (8)
C10	0.00829 (17)	0.0083 (2)	0.00824 (13)	0.00014 (13)	0.00124 (12)	−0.00281 (12)

Cl19	0.01055 (3)	0.01267 (4)	0.00419 (3)	−0.00238 (2)	0.00043 (2)	0.00088 (2)
Cl20	0.00977 (3)	0.00590 (4)	0.00899 (3)	−0.00264 (2)	0.00100 (2)	−0.00102 (2)
Cl25	0.01055 (3)	0.01267 (4)	0.00419 (3)	−0.00238 (2)	0.00043 (2)	0.00088 (2)
Cl26	0.00977 (3)	0.00590 (4)	0.00899 (3)	−0.00264 (2)	0.00100 (2)	−0.00102 (2)
O18	0.01554 (12)	0.00734 (12)	0.00804 (10)	−0.00279 (8)	0.00412 (8)	0.00271 (7)
O24	0.01554 (12)	0.00734 (12)	0.00804 (10)	−0.00279 (8)	0.00412 (8)	0.00271 (7)
C15	0.00864 (11)	0.00526 (15)	0.00569 (10)	−0.00077 (9)	0.00226 (8)	0.00109 (8)
C16	0.00785 (13)	0.00653 (13)	0.00477 (9)	−0.00096 (9)	0.00153 (9)	0.00066 (8)
C17	0.00724 (11)	0.00508 (13)	0.00562 (12)	−0.00116 (8)	0.00150 (9)	0.00025 (9)
C21	0.00864 (11)	0.00526 (15)	0.00569 (10)	−0.00077 (9)	0.00226 (8)	0.00109 (8)
C22	0.00785 (13)	0.00653 (13)	0.00477 (9)	−0.00096 (9)	0.00153 (9)	0.00066 (8)
C23	0.00724 (11)	0.00508 (13)	0.00562 (12)	−0.00116 (8)	0.00150 (9)	0.00025 (9)
Off500ps						
S4	0.01039 (4)	0.00451 (4)	0.00678 (3)	−0.00162 (2)	0.00146 (2)	0.00116 (2)
S5	0.00768 (3)	0.00715 (4)	0.00505 (3)	−0.00060 (2)	0.00119 (2)	0.00080 (2)
S11	0.01039 (4)	0.00451 (4)	0.00678 (3)	−0.00162 (2)	0.00146 (2)	0.00116 (2)
S12	0.00768 (3)	0.00715 (4)	0.00505 (3)	−0.00060 (2)	0.00119 (2)	0.00080 (2)
C1	0.00872 (12)	0.00601 (15)	0.01036 (12)	−0.00113 (9)	0.00194 (9)	−0.00211 (9)
C2	0.01033 (12)	0.00485 (14)	0.00552 (10)	−0.00165 (9)	0.00100 (9)	0.00053 (8)
C3	0.00827 (15)	0.0080 (2)	0.00794 (12)	−0.00012 (12)	0.00127 (11)	−0.00281 (11)
C8	0.00872 (12)	0.00601 (15)	0.01036 (12)	−0.00113 (9)	0.00194 (9)	−0.00211 (9)
C9	0.01033 (12)	0.00485 (14)	0.00552 (10)	−0.00165 (9)	0.00100 (9)	0.00053 (8)
C10	0.00827 (15)	0.0080 (2)	0.00794 (12)	−0.00012 (12)	0.00127 (11)	−0.00281 (11)
Cl19	0.01019 (3)	0.01225 (4)	0.00403 (3)	−0.00232 (2)	0.00043 (2)	0.00083 (2)
Cl20	0.00939 (3)	0.00572 (4)	0.00868 (3)	−0.00257 (2)	0.00098 (2)	−0.00098 (2)
Cl25	0.01019 (3)	0.01225 (4)	0.00403 (3)	−0.00232 (2)	0.00043 (2)	0.00083 (2)
Cl26	0.00939 (3)	0.00572 (4)	0.00868 (3)	−0.00257 (2)	0.00098 (2)	−0.00098 (2)
O18	0.01516 (12)	0.00708 (12)	0.00778 (9)	−0.00276 (8)	0.00407 (8)	0.00263 (7)
O24	0.01516 (12)	0.00708 (12)	0.00778 (9)	−0.00276 (8)	0.00407 (8)	0.00263 (7)
C15	0.00841 (11)	0.00504 (14)	0.00556 (11)	−0.00082 (9)	0.00225 (9)	0.00111 (9)
C16	0.00750 (14)	0.00624 (14)	0.00457 (10)	−0.00108 (10)	0.00139 (9)	0.00054 (8)
C17	0.00712 (11)	0.00488 (13)	0.00549 (12)	−0.00122 (8)	0.00166 (9)	0.00014 (9)
C21	0.00841 (11)	0.00504 (14)	0.00556 (11)	−0.00082 (9)	0.00225 (9)	0.00111 (9)
C22	0.00750 (14)	0.00624 (14)	0.00457 (10)	−0.00108 (10)	0.00139 (9)	0.00054 (8)
C23	0.00712 (11)	0.00488 (13)	0.00549 (12)	−0.00122 (8)	0.00166 (9)	0.00014 (9)

On500ps						
S4	0.01062 (4)	0.00465 (4)	0.00705 (3)	−0.00162 (2)	0.00151 (2)	0.00118 (2)
S5	0.00792 (3)	0.00737 (4)	0.00523 (3)	−0.00060 (2)	0.00118 (2)	0.00081 (2)
S11	0.01062 (4)	0.00465 (4)	0.00705 (3)	−0.00162 (2)	0.00151 (2)	0.00118 (2)
S12	0.00792 (3)	0.00737 (4)	0.00523 (3)	−0.00060 (2)	0.00118 (2)	0.00081 (2)
C1	0.00895 (12)	0.00610 (15)	0.01062 (14)	−0.00109 (9)	0.00196 (10)	−0.00214 (10)
C2	0.01041 (12)	0.00493 (14)	0.00574 (10)	−0.00172 (9)	0.00113 (8)	0.00039 (8)
C3	0.00816 (18)	0.00874 (15)	0.00822 (12)	−0.00038 (12)	0.00121 (12)	−0.00295 (9)
C8	0.00895 (12)	0.00610 (15)	0.01062 (14)	−0.00109 (9)	0.00196 (10)	−0.00214 (10)
C9	0.01041 (12)	0.00493 (14)	0.00574 (10)	−0.00172 (9)	0.00113 (8)	0.00039 (8)
C10	0.00816 (18)	0.00874 (15)	0.00822 (12)	−0.00038 (12)	0.00121 (12)	−0.00295 (9)
Cl19	0.01054 (3)	0.01266 (4)	0.00418 (3)	−0.00238 (2)	0.00045 (2)	0.00086 (2)
Cl20	0.00974 (3)	0.00593 (4)	0.00895 (3)	−0.00263 (2)	0.00099 (2)	−0.00100 (2)
Cl25	0.01054 (3)	0.01266 (4)	0.00418 (3)	−0.00238 (2)	0.00045 (2)	0.00086 (2)
Cl26	0.00974 (3)	0.00593 (4)	0.00895 (3)	−0.00263 (2)	0.00099 (2)	−0.00100 (2)
O18	0.01546 (14)	0.00710 (14)	0.00798 (9)	−0.00262 (10)	0.00418 (9)	0.00271 (8)
O24	0.01546 (14)	0.00710 (14)	0.00798 (9)	−0.00262 (10)	0.00418 (9)	0.00271 (8)
C15	0.00864 (11)	0.00543 (14)	0.00567 (10)	−0.00082 (9)	0.00226 (8)	0.00115 (8)
C16	0.00779 (13)	0.00656 (14)	0.00474 (10)	−0.00105 (9)	0.00136 (9)	0.00066 (8)
C17	0.00729 (11)	0.00495 (14)	0.00564 (11)	−0.00113 (9)	0.00160 (8)	0.00024 (9)
C21	0.00864 (11)	0.00543 (14)	0.00567 (10)	−0.00082 (9)	0.00226 (8)	0.00115 (8)
C22	0.00779 (13)	0.00656 (14)	0.00474 (10)	−0.00105 (9)	0.00136 (9)	0.00066 (8)
C23	0.00729 (11)	0.00495 (14)	0.00564 (11)	−0.00113 (9)	0.00160 (8)	0.00024 (9)
Off800ps						
S4	0.01035 (4)	0.00443 (4)	0.00681 (3)	−0.00165 (2)	0.00146 (2)	0.00114 (2)
S5	0.00762 (3)	0.00712 (4)	0.00504 (3)	−0.00058 (2)	0.00117 (2)	0.00082 (2)
S11	0.01035 (4)	0.00443 (4)	0.00681 (3)	−0.00165 (2)	0.00146 (2)	0.00114 (2)
S12	0.00762 (3)	0.00712 (4)	0.00504 (3)	−0.00058 (2)	0.00117 (2)	0.00082 (2)
C1	0.00851 (14)	0.00587 (15)	0.01050 (12)	−0.00119 (10)	0.00192 (10)	−0.00201 (9)
C2	0.01033 (12)	0.00483 (14)	0.00547 (10)	−0.00178 (9)	0.00108 (9)	0.00047 (8)
C3	0.00799 (18)	0.0080 (2)	0.00785 (14)	0.00027 (13)	0.00111 (13)	−0.00248 (12)
C8	0.00851 (14)	0.00587 (15)	0.01050 (12)	−0.00119 (10)	0.00192 (10)	−0.00201 (9)
C9	0.01033 (12)	0.00483 (14)	0.00547 (10)	−0.00178 (9)	0.00108 (9)	0.00047 (8)
C10	0.00799 (18)	0.0080 (2)	0.00785 (14)	0.00027 (13)	0.00111 (13)	−0.00248 (12)
Cl19	0.01018 (3)	0.01220 (4)	0.00403 (3)	−0.00231 (2)	0.00044 (2)	0.00086 (2)
Cl20	0.00935 (3)	0.00574 (4)	0.00864 (3)	−0.00256 (2)	0.00098 (2)	−0.00098 (2)

Cl25	0.01018 (3)	0.01220 (4)	0.00403 (3)	−0.00231 (2)	0.00044 (2)	0.00086 (2)
Cl26	0.00935 (3)	0.00574 (4)	0.00864 (3)	−0.00256 (2)	0.00098 (2)	−0.00098 (2)
O18	0.01527 (12)	0.00708 (13)	0.00772 (10)	−0.00276 (9)	0.00404 (8)	0.00264 (7)
O24	0.01527 (12)	0.00708 (13)	0.00772 (10)	−0.00276 (9)	0.00404 (8)	0.00264 (7)
C15	0.00838 (12)	0.00524 (15)	0.00545 (10)	−0.00098 (9)	0.00217 (8)	0.00110 (9)
C16	0.00768 (13)	0.00619 (14)	0.00434 (12)	−0.00106 (9)	0.00134 (9)	0.00060 (9)
C17	0.00708 (11)	0.00476 (13)	0.00547 (11)	−0.00112 (8)	0.00167 (8)	0.00022 (8)
C21	0.00838 (12)	0.00524 (15)	0.00545 (10)	−0.00098 (9)	0.00217 (8)	0.00110 (9)
C22	0.00768 (13)	0.00619 (14)	0.00434 (12)	−0.00106 (9)	0.00134 (9)	0.00060 (9)
C23	0.00708 (11)	0.00476 (13)	0.00547 (11)	−0.00112 (8)	0.00167 (8)	0.00022 (8)
On800ps						
S4	0.01060 (3)	0.00460 (4)	0.00705 (3)	−0.00166 (2)	0.00148 (2)	0.00118 (2)
S5	0.00791 (3)	0.00735 (4)	0.00525 (3)	−0.00057 (2)	0.00119 (2)	0.00083 (2)
S11	0.01060 (3)	0.00460 (4)	0.00705 (3)	−0.00166 (2)	0.00148 (2)	0.00118 (2)
S12	0.00791 (3)	0.00735 (4)	0.00525 (3)	−0.00057 (2)	0.00119 (2)	0.00083 (2)
C1	0.00889 (13)	0.00602 (15)	0.01049 (18)	−0.00100 (9)	0.00193 (12)	−0.00193 (11)
C2	0.01047 (12)	0.00490 (14)	0.00570 (11)	−0.00169 (9)	0.00118 (9)	0.00045 (8)
C3	0.00843 (17)	0.0082 (2)	0.00825 (12)	0.00002 (13)	0.00149 (11)	−0.00303 (12)
C8	0.00889 (13)	0.00602 (15)	0.01049 (18)	−0.00100 (9)	0.00193 (12)	−0.00193 (11)
C9	0.01047 (12)	0.00490 (14)	0.00570 (11)	−0.00169 (9)	0.00118 (9)	0.00045 (8)
C10	0.00843 (17)	0.0082 (2)	0.00825 (12)	0.00002 (13)	0.00149 (11)	−0.00303 (12)
Cl19	0.01051 (3)	0.01259 (4)	0.00422 (3)	−0.00236 (2)	0.00044 (2)	0.00089 (2)
Cl20	0.00968 (3)	0.00589 (4)	0.00895 (3)	−0.00262 (2)	0.00101 (2)	−0.00099 (2)
Cl25	0.01051 (3)	0.01259 (4)	0.00422 (3)	−0.00236 (2)	0.00044 (2)	0.00089 (2)
Cl26	0.00968 (3)	0.00589 (4)	0.00895 (3)	−0.00262 (2)	0.00101 (2)	−0.00099 (2)
O18	0.01549 (14)	0.00718 (12)	0.00787 (10)	−0.00282 (9)	0.00403 (10)	0.00271 (7)
O24	0.01549 (14)	0.00718 (12)	0.00787 (10)	−0.00282 (9)	0.00403 (10)	0.00271 (7)
C15	0.00865 (11)	0.00532 (14)	0.00575 (10)	−0.00092 (8)	0.00228 (8)	0.00101 (8)
C16	0.00792 (11)	0.00647 (14)	0.00469 (9)	−0.00106 (9)	0.00155 (8)	0.00068 (8)
C17	0.00725 (11)	0.00515 (13)	0.00568 (10)	−0.00101 (8)	0.00150 (8)	0.00033 (8)
C21	0.00865 (11)	0.00532 (14)	0.00575 (10)	−0.00092 (8)	0.00228 (8)	0.00101 (8)
C22	0.00792 (11)	0.00647 (14)	0.00469 (9)	−0.00106 (9)	0.00155 (8)	0.00068 (8)
C23	0.00725 (11)	0.00515 (13)	0.00568 (10)	−0.00101 (8)	0.00150 (8)	0.00033 (8)
Off1ns						
S4	0.01037 (3)	0.00448 (4)	0.00679 (3)	−0.00164 (2)	0.00147 (2)	0.00113 (2)
S5	0.00766 (3)	0.00711 (4)	0.00503 (3)	−0.00060 (2)	0.00116 (2)	0.00079 (2)

S11	0.01037 (3)	0.00448 (4)	0.00679 (3)	−0.00164 (2)	0.00147 (2)	0.00113 (2)
S12	0.00766 (3)	0.00711 (4)	0.00503 (3)	−0.00060 (2)	0.00116 (2)	0.00079 (2)
C1	0.00860 (15)	0.00595 (14)	0.01034 (13)	−0.00109 (10)	0.00190 (11)	−0.00209 (9)
C2	0.01033 (12)	0.00463 (14)	0.00562 (10)	−0.00162 (9)	0.00108 (9)	0.00050 (8)
C3	0.00815 (17)	0.0080 (2)	0.00786 (13)	0.00017 (13)	0.00115 (12)	−0.00266 (13)
C8	0.00860 (15)	0.00595 (14)	0.01034 (13)	−0.00109 (10)	0.00190 (11)	−0.00209 (9)
C9	0.01033 (12)	0.00463 (14)	0.00562 (10)	−0.00162 (9)	0.00108 (9)	0.00050 (8)
C10	0.00815 (17)	0.0080 (2)	0.00786 (13)	0.00017 (13)	0.00115 (12)	−0.00266 (13)
Cl19	0.01020 (3)	0.01230 (4)	0.00399 (3)	−0.00229 (2)	0.00044 (2)	0.00086 (2)
Cl20	0.00938 (3)	0.00573 (4)	0.00865 (3)	−0.00256 (2)	0.00097 (2)	−0.00098 (2)
Cl25	0.01020 (3)	0.01230 (4)	0.00399 (3)	−0.00229 (2)	0.00044 (2)	0.00086 (2)
Cl26	0.00938 (3)	0.00573 (4)	0.00865 (3)	−0.00256 (2)	0.00097 (2)	−0.00098 (2)
O18	0.01519 (12)	0.00718 (12)	0.00766 (10)	−0.00271 (8)	0.00407 (8)	0.00262 (7)
O24	0.01519 (12)	0.00718 (12)	0.00766 (10)	−0.00271 (8)	0.00407 (8)	0.00262 (7)
C15	0.00836 (12)	0.00501 (15)	0.00554 (11)	−0.00081 (9)	0.00216 (9)	0.00110 (9)
C16	0.00760 (13)	0.00620 (13)	0.00459 (10)	−0.00100 (9)	0.00147 (8)	0.00067 (8)
C17	0.00721 (11)	0.00483 (13)	0.00537 (12)	−0.00117 (8)	0.00162 (9)	0.00015 (9)
C21	0.00836 (12)	0.00501 (15)	0.00554 (11)	−0.00081 (9)	0.00216 (9)	0.00110 (9)
C22	0.00760 (13)	0.00620 (13)	0.00459 (10)	−0.00100 (9)	0.00147 (8)	0.00067 (8)
C23	0.00721 (11)	0.00483 (13)	0.00537 (12)	−0.00117 (8)	0.00162 (9)	0.00015 (9)
On1ns						
S4	0.01064 (4)	0.00468 (4)	0.00705 (3)	−0.00165 (2)	0.00150 (2)	0.00117 (2)
S5	0.00791 (3)	0.00741 (4)	0.00528 (3)	−0.00061 (2)	0.00121 (2)	0.00085 (2)
S11	0.01064 (4)	0.00468 (4)	0.00705 (3)	−0.00165 (2)	0.00150 (2)	0.00117 (2)
S12	0.00791 (3)	0.00741 (4)	0.00528 (3)	−0.00061 (2)	0.00121 (2)	0.00085 (2)
C1	0.00886 (14)	0.00618 (15)	0.01084 (12)	−0.00116 (10)	0.00201 (10)	−0.00213 (9)
C2	0.01044 (12)	0.00492 (14)	0.00572 (11)	−0.00169 (9)	0.00115 (9)	0.00060 (9)
C3	0.00833 (17)	0.0081 (2)	0.00835 (12)	0.00017 (14)	0.00125 (12)	−0.00278 (12)
C8	0.00886 (14)	0.00618 (15)	0.01084 (12)	−0.00116 (10)	0.00201 (10)	−0.00213 (9)
C9	0.01044 (12)	0.00492 (14)	0.00572 (11)	−0.00169 (9)	0.00115 (9)	0.00060 (9)
C10	0.00833 (17)	0.0081 (2)	0.00835 (12)	0.00017 (14)	0.00125 (12)	−0.00278 (12)
Cl19	0.01056 (3)	0.01270 (4)	0.00419 (3)	−0.00238 (3)	0.00043 (2)	0.00090 (2)
Cl20	0.00970 (3)	0.00598 (4)	0.00900 (3)	−0.00265 (2)	0.00100 (2)	−0.00102 (2)
Cl25	0.01056 (3)	0.01270 (4)	0.00419 (3)	−0.00238 (3)	0.00043 (2)	0.00090 (2)
Cl26	0.00970 (3)	0.00598 (4)	0.00900 (3)	−0.00265 (2)	0.00100 (2)	−0.00102 (2)
O18	0.01570 (12)	0.00736 (13)	0.00796 (10)	−0.00270 (9)	0.00417 (8)	0.00273 (8)

|						
O24	0.01570 (12)	0.00736 (13)	0.00796 (10)	−0.00270 (9)	0.00417 (8)	0.00273 (8)
C15	0.00852 (11)	0.00542 (15)	0.00563 (11)	−0.00078 (9)	0.00221 (9)	0.00114 (9)
C16	0.00775 (14)	0.00649 (14)	0.00473 (10)	−0.00103 (10)	0.00141 (9)	0.00066 (8)
C17	0.00743 (11)	0.00497 (13)	0.00558 (13)	−0.00115 (8)	0.00157 (9)	0.00024 (9)
C21	0.00852 (11)	0.00542 (15)	0.00563 (11)	−0.00078 (9)	0.00221 (9)	0.00114 (9)
C22	0.00775 (14)	0.00649 (14)	0.00473 (10)	−0.00103 (10)	0.00141 (9)	0.00066 (8)
C23	0.00743 (11)	0.00497 (13)	0.00558 (13)	−0.00115 (8)	0.00157 (9)	0.00024 (9)
Heated						
S4	0.01132 (4)	0.00523 (4)	0.00789 (3)	−0.00167 (2)	0.00169 (3)	0.00128 (2)
S5	0.00870 (3)	0.00825 (4)	0.00586 (3)	−0.00064 (2)	0.00132 (2)	0.00088 (2)
S11	0.01132 (4)	0.00523 (4)	0.00789 (3)	−0.00167 (2)	0.00169 (3)	0.00128 (2)
S12	0.00870 (3)	0.00825 (4)	0.00586 (3)	−0.00064 (2)	0.00132 (2)	0.00088 (2)
C1	0.00961 (15)	0.00672 (15)	0.01179 (13)	−0.00119 (10)	0.00228 (11)	−0.00232 (10)
C2	0.01079 (13)	0.00547 (14)	0.00642 (11)	−0.00165 (9)	0.00117 (9)	0.00059 (9)
C3	0.00889 (19)	0.00937 (19)	0.00892 (14)	0.00004 (14)	0.00149 (13)	−0.00309 (12)
C8	0.00961 (15)	0.00672 (15)	0.01179 (13)	−0.00119 (10)	0.00228 (11)	−0.00232 (10)
C9	0.01079 (13)	0.00547 (14)	0.00642 (11)	−0.00165 (9)	0.00117 (9)	0.00059 (9)
C10	0.00889 (19)	0.00937 (19)	0.00892 (14)	0.00004 (14)	0.00149 (13)	−0.00309 (12)
Cl19	0.01156 (4)	0.01402 (5)	0.00470 (3)	−0.00261 (3)	0.00051 (2)	0.00095 (2)
Cl20	0.01070 (3)	0.00669 (4)	0.00989 (3)	−0.00285 (2)	0.00108 (2)	−0.00104 (2)
Cl25	0.01156 (4)	0.01402 (5)	0.00470 (3)	−0.00261 (3)	0.00051 (2)	0.00095 (2)
Cl26	0.01070 (3)	0.00669 (4)	0.00989 (3)	−0.00285 (2)	0.00108 (2)	−0.00104 (2)
O18	0.01673 (14)	0.00813 (13)	0.00858 (10)	−0.00302 (9)	0.00441 (9)	0.00285 (8)
O24	0.01673 (14)	0.00813 (13)	0.00858 (10)	−0.00302 (9)	0.00441 (9)	0.00285 (8)
C15	0.00914 (13)	0.00611 (15)	0.00623 (11)	−0.00086 (9)	0.00235 (9)	0.00118 (9)
C16	0.00842 (14)	0.00707 (14)	0.00506 (13)	−0.00095 (10)	0.00138 (10)	0.00077 (9)
C17	0.00784 (11)	0.00574 (14)	0.00633 (12)	−0.00113 (9)	0.00192 (9)	0.00017 (9)
C21	0.00914 (13)	0.00611 (15)	0.00623 (11)	−0.00086 (9)	0.00235 (9)	0.00118 (9)
C22	0.00842 (14)	0.00707 (14)	0.00506 (13)	−0.00095 (10)	0.00138 (10)	0.00077 (9)
C23	0.00784 (11)	0.00574 (14)	0.00633 (12)	−0.00113 (9)	0.00192 (9)	0.00017 (9)

23
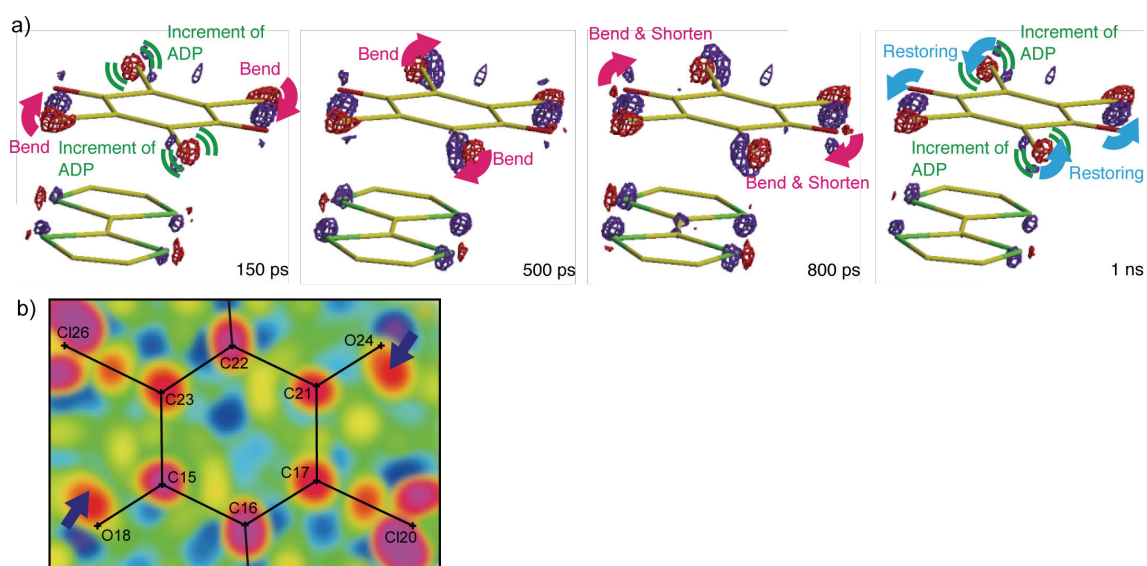
Figure S9. Photo-difference Fourier maps drawn using the reproducibility experimental data. (a) Three-dimensional map. Purple and red surfaces (±0.1 eÅ^{-3} isosurfaces) denote positive and negative electron densities, respectively. (b) Two-dimensional map in the mean plane of CA at Δt = 800 ps (electron density max (blue)/min (red) = 0.08/−0.08 eÅ^{-3}).

References in Supporting Information

[S1] G. M. Sheldrick, *Acta Crystallogr. A* 2008, *64*, 112–122.

[S2] Y. Ozawa, M. R. Pressprich, P. Coppens, *J. Appl. Crystallogr.* 1998, *31*, 128–135.

[S3] P. Coppens, J. Benedict, M. Messerschmidt, I. Novozhilova, T. Graber, Y.-S. Chen, I. Vorontsov, S. Scheinsa, S.-L. Zheng, *Acta Crystallogr., Sect. A* 2010, *66*, 179–188, and references cited therein.

[S4] C. Katan, *J. Phys. Chem. A* 1999, *103*, 1407–1413.